

## Conformation Analysis

## Folding Patterns in a Family of Oligoamide Foldamers

Minna Kortelainen,<sup>[a]</sup> Aku Suhonen,<sup>[a]</sup> Andrea Hamza,<sup>[b]</sup> Imre Pápai,<sup>\*,[b]</sup> Elisa Nauha,<sup>[a]</sup> Sanna Yliniemelä-Sipari,<sup>[a]</sup> Maija Nissinen,<sup>\*,[a]</sup> and Petri M. Pihko<sup>\*,[a]</sup>

**Abstract:** A series of small, unsymmetrical pyridine-2,6-dicarboxylamide oligoamide foldamers with varying lengths and substituents at the end groups were synthesized to study their conformational properties and folding patterns. The @-type folding pattern resembled the oxyanion-hole motifs of enzymes, but several alternative folding patterns could also be characterized. Computational studies revealed several alternative conformers of nearly equal stability. These folding patterns differed from each other in their intramolecular hydrogen-bonding patterns and aryl–aryl interactions. In the

solid state, the foldamers adopted either the globular @-type fold or the more extended S-type conformers, which were very similar to those foldamers obtained computationally. In some cases, the same foldamer molecule could even crystallize into two different folding patterns, thus confirming that the different folding patterns are very close in energy in spite of their completely different shapes. Finally, the best match for the observed NOE interactions in the liquid state was a conformation that matched the computationally characterized helix-type fold.

## Introduction

The oxyanion hole is perhaps one of the most studied motifs in the active sites of enzymes.<sup>[1,2]</sup> Oxyanion holes stabilize high-energy intermediates and transition states that bear negatively charged oxygen atoms in enzymatic reactions that involve tetrahedral intermediates (e.g., hydrolytic cleavage reactions of (thio)esters and amides) and reactions that involve enolate intermediates.<sup>[2]</sup> In both cases, a charge builds up on the carbonyl oxygen atom on the way to a negatively charged intermediate, such as a tetrahedral intermediate or an enolate ion.<sup>[2]</sup>

In the realm of small-molecule catalysis, hydrogen-bond donors, such as (thio)urea and squaramide functionalities, could be viewed as analogues of the oxyanion holes.<sup>[3]</sup> These functionalities are relatively rigid and flat two-point hydrogen-bond donors. In contrast, the oxyanion holes in enzymes are

three-dimensional, with two, or even three, hydrogen-bond donors that stabilize the charge at the oxyanion. The hydrogen-bond donors that comprise the oxyanion hole are separated by rotatable bonds of the amino acids. As such, mimicking the hydrogen-bond donor patterns of oxyanion holes with simple peptides might be extremely challenging due to the flexibility of the peptide backbone. However, peptide-type foldamers<sup>[4]</sup> that bear more rigid subunits<sup>[5]</sup> might offer better possibilities for folding into oxyanion-hole-type conformations. A variety of rigid aromatic oligomers composed of, for example, pyridine-2,6-carboxamide,<sup>[6]</sup> anthranilamide,<sup>[7]</sup> quinoline,<sup>[8]</sup> quinoxaline,<sup>[9]</sup> and other aryl–amide monomers,<sup>[10]</sup> have been studied since the 1990s. Still, only scattered examples of non-peptidic structures in which amide or ester carbonyl groups act as multiple hydrogen-bond acceptors have previously been described,<sup>[11]</sup> and foldamers that bear oxyanion-hole-type structures have not been systematically studied at all. In the previous examples of oligomers, the emphasis was placed on control of the folding properties, governed mainly by the repeating hydrogen-bond patterns<sup>[5–10]</sup> and aromatic interactions, which were adjusted by varying the functionalization of the aromatic rings.<sup>[10a]</sup> In many cases, the foldamers also contained an interior cavity of varying size at the center of the fold instead of a tight fold stabilized by multiple interactions.<sup>[5c–e]</sup>

Herein, we show that simple unsymmetrical pyridine-2,6-dicarboxylamide-derived oligoamides can adopt several alternative conformers (folding patterns, or in short folds) of nearly equal stability. Importantly, one of these conformers, observed in both the solid and liquid states, has two or even three NH groups hydrogen bonded to the terminal amide carbonyl group, thus closely resembling an oxyanion-hole motif. Although the amide carbonyl group is not an oxyanion in the classical Lewis sense, it is important to note that the oxygen

[a] M. Kortelainen,<sup>+</sup> A. Suhonen,<sup>+</sup> Dr. E. Nauha, Dr. S. Yliniemelä-Sipari, Prof. Dr. M. Nissinen, Prof. Dr. P. M. Pihko  
Department of Chemistry, Nanoscience Center  
University of Jyväskylä  
P.O. Box 35, 40014 JYU (Finland)  
Fax: (+358) 14-260-2501  
E-mail: papai.imre@ttk.mta.hu  
maija.nissinen@jyu.fi  
petri.pihko@jyu.fi

[b] Dr. A. Hamza, Dr. I. Pápai  
Institute of Organic Chemistry  
Research Center for Natural Sciences  
Hungarian Academy of Sciences  
Magyar Tudósok Körútja 2, 1117, Budapest (Hungary)

[<sup>+</sup>] These authors contributed equally to this work.

Supporting information for this article is available on the WWW under <http://dx.doi.org/10.1002/chem.201406521>.

atom of the amide carbonyl unit already bears a substantial charge; that is, the net atomic charge ( $Q(O)$ ) in *N*-methylacetamide is  $-0.65$ , whereas the corresponding value for *S*-methylthioacetate enolate is  $-0.77$ .<sup>[12]</sup> In other words, the amide group can be viewed at least as a crude mimic of the enolate anion.<sup>[12]</sup> As such, the search for foldamers that can stabilize oxyanions might well start with systems that bear an amide group that is intramolecularly hydrogen bonded through its carbonyl oxygen atom to multiple hydrogen-bond donors.

The point of departure of the present study was the single-crystal X-ray structure previously described by three of us,<sup>[13]</sup> in which one of the amide carbonyl groups is hydrogen bonded to three other amide NH groups (Figure 1). The structure of

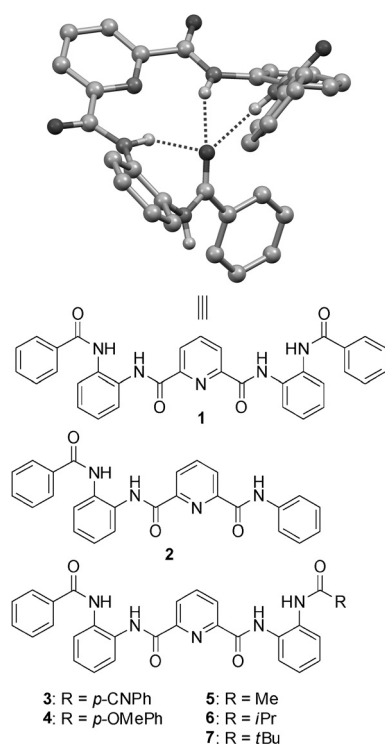


**Figure 1.** Structure of foldamer 1<sup>[13]</sup> and schematic presentation of unsymmetrical derivatives 2–7. The solvated EtOH molecule and non-hydrogen-bonding hydrogen atoms have been omitted for clarity from the X-ray structure (top).

1 raised hopes that similar motifs could be used as triple hydrogen-bonding oxyanion-hole motifs,<sup>[3b]</sup> but the stability and possibility of alternate conformers that were energetically as favorable have remained open questions. To address these questions, we embarked on a more comprehensive study of a family of foldamers, including the original foldamer 1. By using a combination of computational and X-ray crystallographic studies, we show that 1 and related asymmetric foldamers 2–7 indeed adopt structures similar to the original structure of 1, but alternate folds that are close in energy in the gas phase can also be experimentally characterized.

## Results and Discussion

The present study involved the synthesis of unsymmetrical oligopeptide foldamers 2–7, conformational analysis of the foldamers by means of computational studies, and structural characterization by X-ray crystallography and solution-phase NMR spectroscopic measurements.

### Synthesis of unsymmetrical foldamers

For the synthesis of unsymmetrical foldamers 2–7, monofunctionalized versions of the core building blocks pyridine-2,6-dicarboxylic acid and 1,2-diaminobenzene 8 were required (see Scheme 1). Monoprotected pyridine-2,6-dicarboxylic acid 14 was readily prepared by using the method developed by Schmuck and Machon.<sup>[14]</sup> Monoacylation of 8 could be achieved directly with HOBt/EDC coupling, but better results were obtained for aliphatic carboxylic acids when 2-nitroaniline 11 was used as a starting material (alternative 1, Scheme 1), followed by reduction of the resulting nitroanilide 12. Standard HOBt/EDC coupling reactions could be used to assemble the oligoamide framework from 14 and 10 in two steps (Scheme 1).

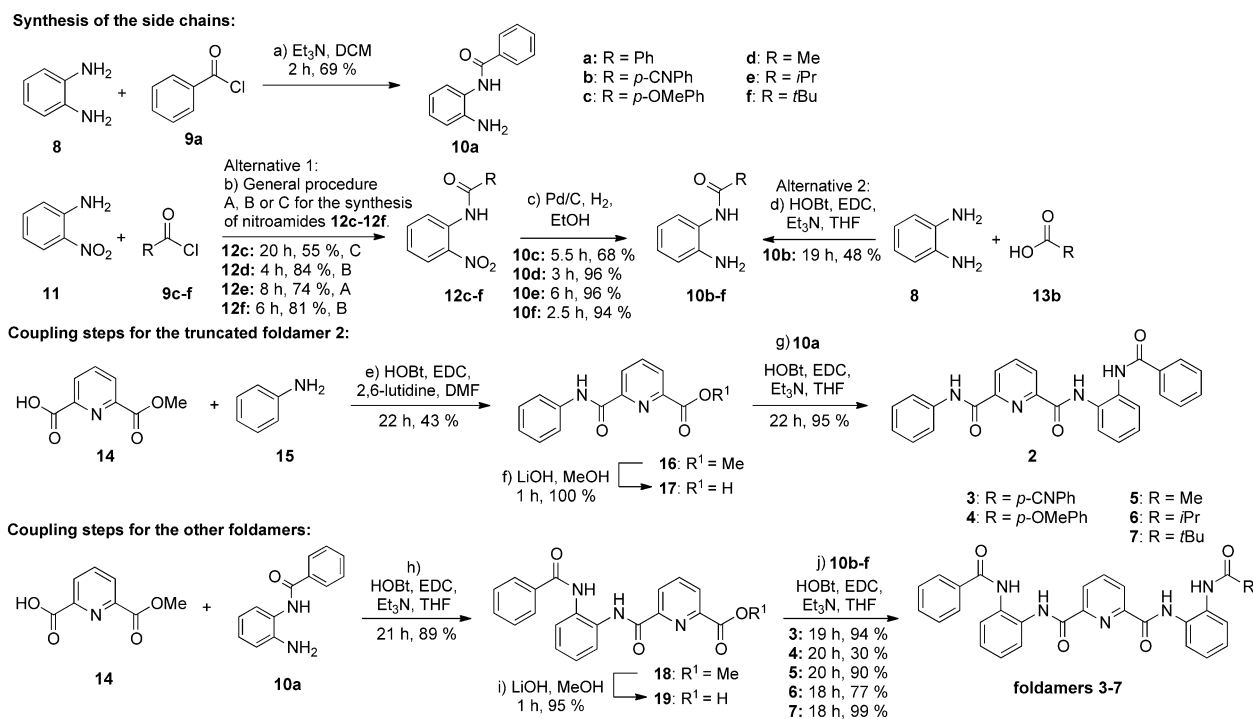
Six different unsymmetrical foldamers were synthesized. The simplest foldamer 2 possessed only three amide linkages instead of four (Figure 1). Others were variants of 1 ( $R = \text{Ph}$ ) with different side chains, namely, two different aryl rings ( $R = p\text{-NC-Ph}$  (3) and  $p\text{-OMe-Ph}$  (4)) and three different aliphatic side chains ( $R = \text{Me}$  (5),  $R = i\text{Pr}$  (6), or  $R = t\text{Bu}$  (7)) to probe the electronic and steric effects of the folding process.

### Computational studies

A computational analysis for a set of foldamers was performed with the main aim of identifying the nature of the stabilizing interactions that govern the conformational distribution of these compounds. An extensive conformational search was carried out by using a combination of MM and DFT methods. Geometry optimizations, vibrational analysis, and an estimation of the solvent effects were carried out at the  $\omega\text{B97X-D/6-311G(d,p)}$  level of theory; however, the electronic energies were further refined by additional single-point-energy calculations with the extended 6-311++G(3df,3pd) basis set. The relative stabilities were analyzed in terms of gas-phase Gibbs free energies. Further details of the applied methodology are provided in the Computational Approach section.

Three different conformers (folds) could be computationally identified for the simplest truncated foldamer 2. The optimized structures and their relative stabilities are shown in Figure 2. For the clarity of further discussion, the identified folds were classified as follows:

- 1) The fold in which the outer carbonyl group serves as a hydrogen-bond acceptor, that is, a focal point around which the rest of the structure folds, is called the @-fold.
- 2) The fold in which the hydrogen-bond formed between an inner carbonyl group and the adjacent amide NH unit en-



**Scheme 1.** Synthesis of unsymmetrical foldamers 2–7 (see the Experimental Section for details). EDC = *N*-(3-dimethylaminopropyl)-*N*-ethylcarbodiimide, HOBt = 1-hydroxybenzotriazole.

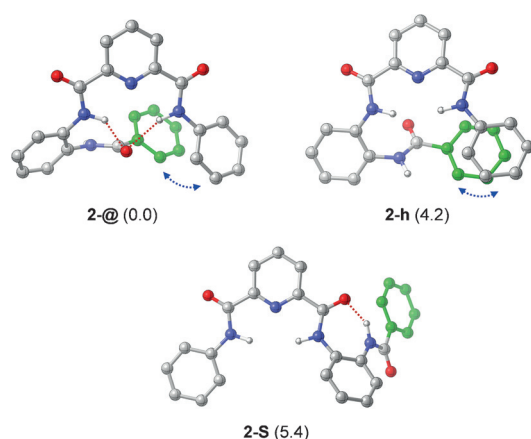


**Figure 2.** Optimized structures of the conformers identified computationally for foldamer 2. The relative stabilities are shown in parenthesis (in kcal mol<sup>-1</sup>). Intramolecular hydrogen bonds are indicated by dotted lines and aromatic interactions are highlighted by blue arrows. The CH hydrogen atoms have been omitted for clarity. Note: hydrogen bonds to the pyridine nitrogen atoms have been omitted for clarity in all the structures.

forces a turn that results in an S-shaped molecule is called the S-fold.

3) The remaining conformer is referred to as an h-fold based on its helical shape.

Conformer 2-@ is predicted to be the most stable form, which is clearly separated from the other two forms in free energy. This structure is stabilized by a double hydrogen bond.

The van der Waals contact between the terminal phenyl groups is also apparent, but the aromatic rings are somewhat displaced from the optimal parallel arrangement. No hydrogen bonds are present in structure 2-h, which lies 4.2 kcal mol<sup>-1</sup> above 2-@ in free energy. This structure is stabilized by aromatic-stacking interactions. In the third structure (2-S), only a single hydrogen bond that involves one of the inner carbonyl groups provides intramolecular stabilization. Conformer 2-S is computed to be at 5.4 kcal mol<sup>-1</sup> in free energy.

For the symmetrical foldamer 1, four different low-lying conformers that feature multiple hydrogen bonds and aromatic interactions could be identified (Figure 3). The structures of 1-S, 1-@, and 1-@' are analogous to 2-@ in the central hydrogen-bonding pattern, but 1-S has a turn as a result of a terminal hydrogen bond. The two @ conformers (1-@ and 1-@') have very similar folded shapes, but they differ in the number of hydrogen bonds (i.e., three and two, respectively) and also in the orientation of the terminal phenyl groups. Conformer 1-h can be derived from 2-h. Calculations predict 1-S to be the most favored form; however, the other conformers are at the most 1.3 kcal mol<sup>-1</sup> less stable. Aryl-aryl interactions seem to provide additional stabilization in all these structures (highlighted in Figure 3). In conformer 1-h, both terminal phenyl groups are involved in an aromatic-stacking interaction that results in a compact helix structure that lies only 0.4 kcal mol<sup>-1</sup> above 1-S. Unlike in structure 2-h, hydrogen-bonding interactions can also be identified in conformer 1-h. An additional conformer with two turns that lead to a W-shape structure could also be located on the potential-energy surface (1-W in Figure 3). This conformer is far less stable than the other forms, which is relat-

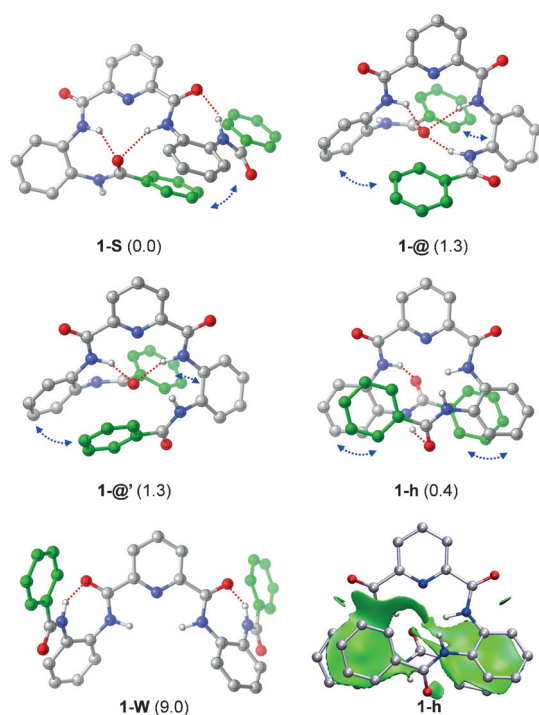


**Figure 3.** Optimized structures of the conformers identified computationally for foldamer 1 and an NCI plot generated for structure **1-h**. Characteristic van der Waals contacts are represented by the green regions. An applied cutoff for the gradient is 0.3 au.

ed to the absence of oxyanion-type hydrogen-bonding and aromatic-stacking interactions in **1-W**.

Thus, these computational results confirm that the conformational distribution of oligoamides **1** and **2** is primarily governed by N–H...O type hydrogen bonds, but these results also point to stabilizing effects due intramolecular van der Waals contacts between the aromatic rings. For an illustration of these latter noncovalent interactions (NCIs), we generated a reduced gradient (RDG) isosurface plot for structure **1-h** by using the method developed by Yang and co-workers.<sup>[15,16]</sup> The NCI plot depicted in Figure 3 indeed displays broad contact areas between the interacting aryl groups.

The strength and the balance of these noncovalent forces can be notably altered by introducing various substituents at the *para* position of the terminal phenyl group, as exemplified by foldamers **3** and **4**. The conformers of molecules **3** and **4** were derived from the conformers of the symmetrical foldamer **1**, and these conformers were all subjected to geometry optimization. Each conformer of **1** gives rise to a pair of folds that differ in the position of the substitution. Thus, additional labeling to distinguish the two types of unsymmetrical conformer is introduced: labels  $S_1$ ,  $@_1$ ,  $@'_1$ , and  $h_1$  refer to conformers in which the carbonyl oxygen atom adjacent to the substituted phenyl end serves as the central hydrogen-bond acceptor, whereas  $S_2$ ,  $@_2$ ,  $@'_2$ , and  $h_2$  correspond to conformers in which the hydrogen-bond acceptor is next to the unsubstituted phenyl group. The relative stabilities of these two conformers may vary appreciably, as shown by the relative Gibbs free energies of various conformers for foldamers **1**, **3**, and **4** in Table 1.

Table 1. Relative stabilities of various forms of foldamers <b>1</b> , <b>3</b> , and <b>4</b> . <sup>[a]</sup>			
Conformers	Foldamer 1	Foldamer 3	Foldamer 4
S	0.0	0.0 ( $S_2$ ) 2.5 ( $S_1$ )	0.0 ( $S_1$ ) 1.6 ( $S_2$ )
@	1.3	3.4 ( $@_2$ ) – <sup>[b]</sup>	2.5 ( $@_1$ ) 3.4 ( $@_2$ )
@'	1.3	0.7 ( $@'_2$ ) 3.3 ( $@'_1$ )	2.4 ( $@'_2$ ) 2.4 ( $@'_1$ )
h	0.4	0.2 ( $h_1$ ) 1.4 ( $h_2$ )	0.9 ( $h_2$ ) 1.2 ( $h_1$ )

[a] Reported data are relative Gibbs free energies (in kcal mol<sup>-1</sup>) with respect to the most stable conformer. [b] Only a single structure could be identified computationally in this particular case (optimization converged to conformer **3-h** for the other structural variant).

For instance, the preferred conformer for foldamer **3** is **3-S<sub>2</sub>**, with a cyano group on the phenyl ring that does not take part in the aryl–aryl interaction (Figure 4). The alternative folding pattern (i.e., **3-S<sub>1</sub>**) with a cyano group at the opposite terminus yields a less stable structure by 2.5 kcal mol<sup>-1</sup>. On the other hand, the order of relative stabilities of these two conformers is reversed for foldamer **4**, and these stabilities differ by 1.6 kcal mol<sup>-1</sup> (**4-S<sub>1</sub>** is shown in Figure 4). The observed variations in the relative stabilities of these conformers can be associated with the electronic properties of the CN and OMe substituents, which strengthen or weaken the hydrogen-bonding interactions in the proximity of the substituents and likely affect the nature of the aromatic interactions as well. Similar effects are also expected for the other classes of fold. Interestingly, the  $@_1$ -type conformer of foldamer **3** is spontaneously transformed into conformer **3-h<sub>1</sub>** upon geometry optimization, and its structural counterpart (i.e., **3-@<sub>2</sub>**) is predicted to be relatively high in free energy (at 3.4 kcal mol<sup>-1</sup>).

Computational studies were carried out for foldamers **5** and **7** with methyl and *tert*-butyl groups replacing one of the terminal phenyl groups in foldamer **1**, respectively. The geometry optimizations indeed yielded structures analogous to **1** (Figure 4). The conformers of unsymmetrical foldamers **5** and **7** can be classified into the same categories as introduced above. Thus, the fold labels  $S_1$ ,  $@_1$ ,  $@'_1$ , and  $h_1$  refer to conformers in which the carbonyl group next to the Ph→R replacement is involved in the central hydrogen-bonding interaction, and  $S_2$ ,  $@_2$ ,  $@'_2$ , and  $h_2$  refer to folds in which the hydrogen-bond acceptor is next to the unsubstituted phenyl group.

The computational data also reveal that the  $S_2$  conformers are the most stable forms of these foldamers, but the other folds are typically higher in free energy by only 1–2 kcal mol<sup>-1</sup> (Table 2). On the basis of the electron-donating nature of the Me and *t*Bu alkyl groups, particular stabilization for conformers with these groups next to the central hydrogen-bonding pattern is expected. This outcome is indeed the case for  $@$ -conformers (the  $@_1$  forms are favored). However, the computational studies predict the  $S_2$  and  $@'_2$  variants to be more favorable for the S and  $@'$  folds (Figure 4). These results suggest that the electronic-stabilization effects are counterbalanced by the loss of the aromatic interactions upon the Ph→R replacement. The

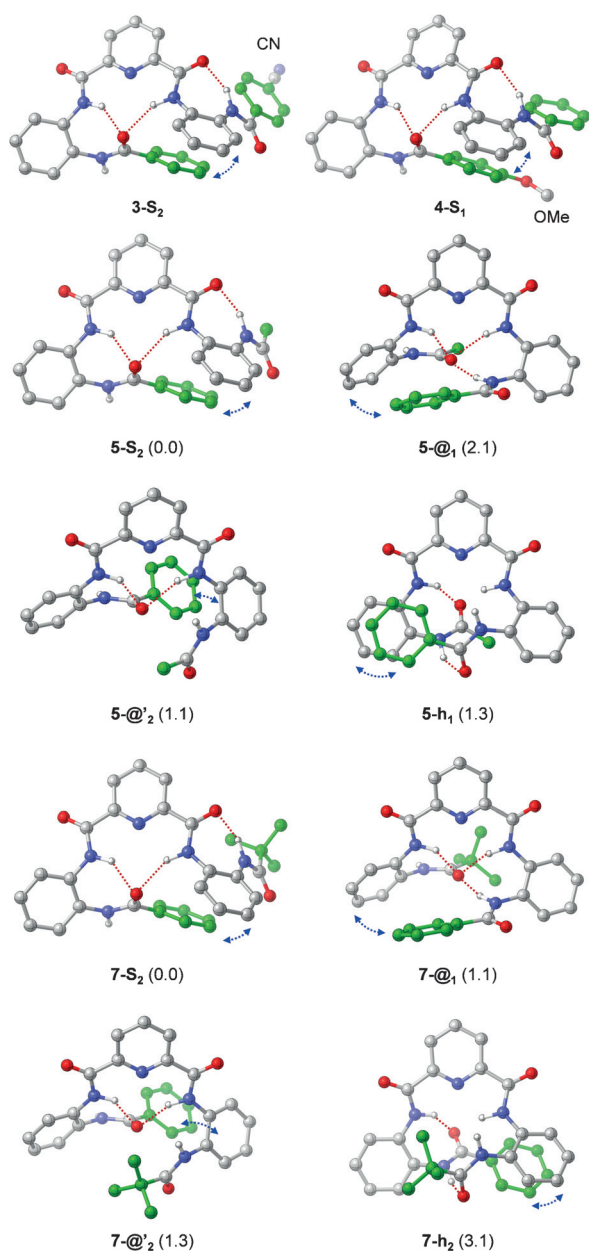


Figure 4. Most stable conformers of foldamers 3-5 and 7.

Table 2. Relative stabilities of various forms of foldamers 1, 5, and 7. <sup>[a]</sup>			
Conformers	Foldamer 1	Foldamer 5	Foldamer 7
S	0.0	0.0 (S <sub>2</sub> ) 2.0 (S <sub>1</sub> )	0.0 (S <sub>2</sub> ) 1.2 (S <sub>1</sub> )
@	1.3	2.1 (@ <sub>1</sub> ) 2.7 (@ <sub>2</sub> )	1.1 (@ <sub>1</sub> ) 1.8 (@ <sub>2</sub> )
@'	1.3	1.1 (@' <sub>2</sub> ) 2.2 (@' <sub>1</sub> )	1.3 (@' <sub>2</sub> ) 1.5 (@' <sub>1</sub> )
h	0.4	1.3 (h <sub>1</sub> ) 2.2 (h <sub>2</sub> )	2.3 (h <sub>2</sub> ) 3.1 (h <sub>1</sub> )

[a] Reported data are relative Gibbs free energies (in kcal mol<sup>-1</sup>) with respect to the most stable conformer.

relative stabilities of the less favored conformers of 5 and 7 vary only slightly with respect to those of the original symmetrical molecule and stay within a narrow energy range relative to the most stable forms.

### Solid-state conformations

Single-crystal structures were obtained for all the foldamers, except for the methoxyphenyl derivative 4. For foldamers 2, 3, and 6, both structures with the @ and S conformers were obtained equally by crystallization under various conditions (Table 3 and Figure 5). Although computational studies

Table 3. Conformers of foldamers 1-7 in the XRD structures.<sup>[a]</sup>

Foldamer	@ Conformation	S Conformation
1 <sup>[13]</sup>	1-@ <sub>2</sub> -EtOH	-
2	2-@-Form I 2-@-S-DMF	2-S-MeCN
3	3-@ <sub>2</sub> -Form I	3-S <sub>1</sub> -EtOAc
4	-	-
5	-	5-S <sub>1</sub> -Form I
6	6-@ <sub>2</sub> -Form I	6-S <sub>1</sub> -Form II
7	-	7-S <sub>2</sub> -Form I

[a] Forms I and II denote polymorphic crystal forms and a solvent molecule indicates a solvate structure.

showed only a slight difference in stability toward the h conformation, the latter was not observed in the solid state. Typically, the @ conformer was obtained in unsolvated structures with no solvent included in the crystal lattice, whereas the S conformer was observed both in the solvates and unsolvated structures, with a preference for the solvates.

The solid-state conformers are very similar to those conformers identified computationally. This finding can be visually assessed from the overlay structures (Figure 5 a, e, and j), in which the computationally derived and X-ray structures display closely related geometries and hydrogen-bonding patterns.<sup>[17]</sup> Similar to the computed structures, the @ conformers are each stabilized by two or three hydrogen bonds to the C=O group of the outer phenyl ring. The S conformers are always stabilized by an intramolecular hydrogen bond between an outer NH group and an inner C=O group. Additionally, two intramolecular hydrogen bonds to a C=O group of the outer phenyl ring contribute to the stability of the S fold, except for the truncated foldamer 2, in which such hydrogen bonding is not possible. The biggest difference in the computational and crystal structures is seen in the aryl-aryl interactions of the @ conformers, which played a significant role in the computational structures. In the solid state, however, intramolecular aryl-aryl interactions, although present, are not as significant (see the overlay in Figure 5 a, j for examples).

In general, the folds observed in the solid state are slightly looser relative to those folds obtained computationally. This situation could either be related to crystal-packing forces or

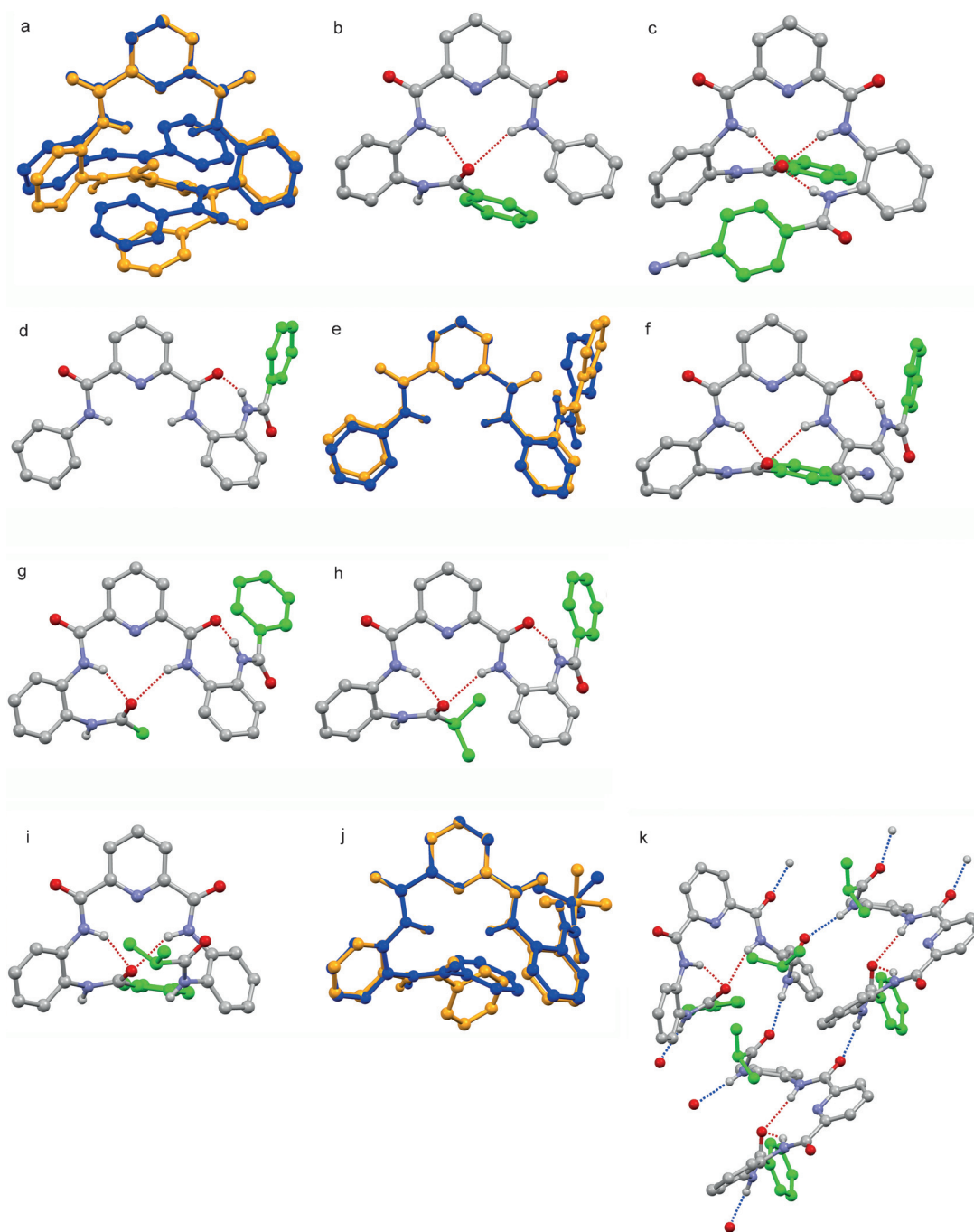


**Figure 5.** First row: a) An overlay structure of the calculated @ conformation (blue; see Figure 3) and the @ conformation in the XRD structure of an EtOH solvate of foldamer 1 (orange, from reference [6a]), b) XRD structure of foldamer 2 in the @ conformation (2-@-Form I), c) XRD structure of foldamer 3 in the @<sub>2</sub> conformation (3-@<sub>2</sub>-Form I). Second row: d) XRD structure of foldamer 2 in the S conformation (2-S-MeCN), e) an overlay structure of the calculated S-conformation (2-S, blue; see Figure 2) and the XRD structure of foldamer 2 in the S conformation (2-S-MeCN, orange), and f) XRD structure of foldamer 3 in the S<sub>1</sub> conformation (3-S<sub>1</sub>-EtOAc). Third row: XRD structures of g) foldamer 5 in the S<sub>1</sub> conformation (5-S<sub>1</sub>-Form I), h) foldamer 6 in the S<sub>1</sub> conformation (6-S<sub>1</sub>-Form II). Fourth row: i) foldamer 6 in the @ conformation (6-@<sub>2</sub>-Form I), and j) an overlay structure of the calculated S<sub>2</sub> conformation (7-S<sub>2</sub>, blue; Figure 2) and XRD structure of foldamer 7 in the S<sub>2</sub> conformation (7-S<sub>2</sub>-Form I, orange), k) crystal-packing structure of foldamer 6 in the @<sub>2</sub> conformation (6-@<sub>2</sub>-Form I). The intramolecular hydrogen bonds are presented in red and the intermolecular hydrogen bonds in blue. The non-amide hydrogen atoms and hydrogen bonds to the pyridine nitrogen atoms have been omitted for clarity.

the present computational method may slightly overestimate the strength of the aryl–aryl interactions. In analogy with the computationally identified structures, two different types of S conformer could also be characterized in the solid state, whereas the @ conformers were always of the @<sub>2</sub> type.

In the solid-state structures obtained so far, foldamer 1 always adopted the standard @ conformer (Figure 5).<sup>[13]</sup> The aromatic interactions described in the calculations are also seen in the solid-state structure of 1, but the relative positions of the interacting aryl groups are different (i.e., the distances

of the centroids are fairly long; see Figure 5 a and the Supporting Information).

The truncated foldamer **2**, a special case among the series due to its diminished hydrogen-bonding possibilities, can still adopt both @ and S conformations in the solid state (Figure 5), although calculations indicate a preference for the @ conformation. In the calculated structure, the orientation of the end aryl groups is slightly displaced parallel, whereas the orientation in the solid state is T-shaped.<sup>[11]</sup>

Interestingly, foldamer **2** was the only foldamer that crystallized with both the @ and S conformer appearing within the same crystal structure. This scenario suggests that foldamer **2** is likely to populate both conformations in a solution in significant proportions.

As expected, the @<sub>2</sub> conformer is observed in the unsolvated crystal structure of foldamer **3** due to the electron-withdrawing cyano substituent (Figure 5). The aryl–aryl interactions within the @<sub>2</sub> conformer of **3** are very weak (Figure 5 c). Although the computations predict that the S<sub>2</sub> fold is more stable for **3** than S<sub>1</sub> (Table 1), the S<sub>1</sub> conformer appears to be more accessible in the solid state (Table 3, entry 3) possibly because of the effect of the solvent in the crystal lattice; that is, two molecules of foldamer **3** adopt the S<sub>1</sub> fold and form a pair with a void big enough for partial solvent inclusion. This particular crystal form seems to be very stable because altogether four isomorphous solvate structures (in EtOAc, THF, CHCl<sub>3</sub>, and DMA) have been obtained so far.<sup>[18]</sup>

Acetyl foldamer **5** also seems to prefer the S<sub>1</sub> fold in the solid state exclusively (Figure 5), even in the unsolvated form, although the computational studies again predicted that the S<sub>2</sub> conformer is slightly more stable (see Table 2 and Figure 4). However, the energy difference in the computational results was relatively small (2 kcal mol<sup>-1</sup>), thus indicating that these conformations are almost equally stable and that environmental factors during the crystallization may drive the conformation to either fold.

Isopropyl foldamer **6** crystallized as two unsolvated polymorphs, one with a loose @<sub>2</sub> conformer and one that adopted an S<sub>1</sub> conformer (Figure 5). In contrast to the other @ conformers, the @<sub>2</sub> conformer of **6** has only two intramolecular hydrogen bonds to a central hydrogen-bond acceptor. The third hydrogen bond from the outer amide group makes an intermolecular hydrogen bond to the adjacent molecule of **6**. This interaction may be because of a more efficient crystal-packing mode or because of the relatively large size of the isopropyl group, which prohibits tighter folding due to steric hindrance with one of the inner benzene rings. Aromatic interactions are also observed, but the distances are also fairly long in this case (Figure 5 i). In the polymorphic structure of foldamer **6** with an S<sub>1</sub> conformer, there is no significant steric hindrance and the electron-rich carbonyl oxygen atom near the isopropyl group can form the two intramolecular hydrogen bonds.

The *tert*-butyl foldamer **7** was the only foldamer that crystallized with an S<sub>2</sub> conformer (Figure 5), which is in agreement with the computational studies. The crystal packing of this structure consists of molecular chains, and the large *tert*-butyl group fits better at the outer edge of the molecule in the S<sub>2</sub>

conformer in this packing structure, whereas the large *tert*-butyl group in the inner part of the molecule in the S<sub>1</sub> conformer would hinder the formation of the intramolecular hydrogen-bonding network that is important to the stability of the packing structure.

In conclusion, the foldamers generally adopt solid-state conformers that are remarkably similar to those obtained in the computational studies. Interestingly, many of the foldamers (i.e., **2**, **3**, and **6**) crystallized in both @- and S-folded conformers, thus indicating that it is likely that both of these conformers are also present in solution and that the environment during the crystallization affects which conformer is formed in the solid state.

### Solution-state studies (NMR)

For the solution-state studies, foldamer **5** was selected as a probing compound due to its good solubility in CDCl<sub>3</sub> and clear <sup>1</sup>H NMR spectrum with a well-separated CH<sub>3</sub> singlet from the aromatic and the N–H signals. Foldamers **1–4** only have good solubility in solvents with good hydrogen-bond donation (such as DMF or DMSO), and these solvents might disrupt the intramolecular hydrogen bonds of some of the folds.

The 2D NOESY and 1D NOE experiments of **5** in CDCl<sub>3</sub> clearly showed that the methyl protons correlate to all four N–H signals, whereas no correlation between the N–H groups and the pyridine ring was observed (see the Supporting Information for details). This finding indicates that a conformer in which all the N–H groups face inside the folded molecule, most likely an @ or h conformer, is populated in solution. In the S conformer, one of the N–H groups is too far from the methyl group to display a correlation with the CH<sub>3</sub> group.

NOE interactions show the best match of the computationally derived h conformer with a nonplanar arrangement of the three central aryl groups (Figure 6) because most of the correlations match well, and even the distances for the N–H–methyl group are in the correct order based on the observed NOE interactions (Table 4). These results indicate that, at least in CDCl<sub>3</sub>, the acetyl foldamer seems to favor the h-like conformer or there is constant conformational variation in solution between the @, S, and other conformers, and that the averaged structure, on the NMR timescale, matches best with the h-like conformer. Such a conformational variation would

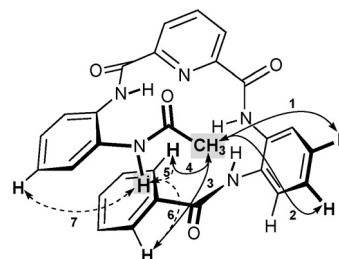


**Figure 6.** Schematic representation of the acetyl foldamer **5** in the h conformation. Key diagnostic NOE interactions of the acetyl CH<sub>3</sub> group (solid arrows) and from the acetamide N–H group (dashed arrows) are shown.

Table 4. Calculated key diagnostic NOE distances of <b>5</b> <sup>[a]</sup> and experimental NOE enhancement.		
NOE interaction	C–H...H–N/H <sub>3</sub> C [Å] <sup>[b]</sup>	NOE enhancement [%] <sup>[c]</sup>
1	4.628	0.08 <sup>[d]</sup>
2	4.606	0.08 <sup>[d]</sup>
3	4.758	0.05 <sup>[e]</sup>
4	4.635	0.05 <sup>[e]</sup>
5	3.208	0.95 <sup>[f]</sup>
6	3.979	0.95 <sup>[f]</sup>
7	4.610	0.52

[a] h conformer; see Figure 4. [b] The shortest distance to a Me hydrogen atom has been used when measuring the distances [c] See Figure 6 for labeling of the NOE interactions. [d]–[f] Same peaks.

enable the crystallization of the acetyl foldamer **5** in the S<sub>1</sub> conformation.

## Conclusion

We have described herein the folding patterns of seven different oligoamide foldamers based on a 2,6-pyridinedicarboxamide core. In spite of seemingly minute variations in their structures, these foldamers have exhibited a remarkable variety in their folding patterns, as seen in the computationally derived gas-phase structures and in the solid-phase structures obtained by X-ray crystallography studies. Two major folds were identified in the gas and solid phases, the compact @ fold, which resembles an oxyanion-hole motif, and the more extended S fold. Both of these folds were characterized by three intramolecular hydrogen bonds. For some foldamers, both the @- and S-folded conformers could be characterized in the solid state, thus providing experimental confirmation that these conformers are close in energy. The computationally derived energies of these two folds were also within 1–2 kcal mol<sup>-1</sup> for most of the foldamers. A third h fold, a helix, was characterized in the computational studies and was a likely alternative in solution for foldamer **5** with an N-acetyl terminus. Computational studies indicated that both hydrogen bonds and dispersion interactions (aryl–aryl or aryl–alkyl) are responsible for the stability of these folds. However, the aryl–aryl interactions in the crystal structures appear to be less significant, thus causing slightly looser conformers.

The fact that these conformationally very distinct folds are computationally so close in energy suggests that these foldamers could be used as conformational switches because they can readily attain at least two stable states. Studies toward understanding the dynamics of the folding and the effects of further substitution are in progress.

## Experimental Section

All the reactions were carried out in an argon atmosphere in oven-dried glassware, except for the hydrolytic reactions. When needed, nonaqueous reagents were transferred under argon by syringe or cannula and dried prior to use. Dichloromethane, THF, and toluene

were obtained by passing deoxygenated solvents through activated alumina columns (MBraun SPS-800 Series solvent purification system). MeOH, DMF, and pyridine were distilled and placed over molecular sieves (4 Å). The EtOH used in reduction reactions with Pd/C was placed over molecular sieves (4 Å). Other solvents and reagents were used as obtained from the supplier. Analytical TLC was performed on Merck silica gel 60 F<sub>254</sub> (230–400 mesh) plates and analyzed with UV light and staining by heating with vanillin solution (vanillin (2.4 g), conc. H<sub>2</sub>SO<sub>4</sub> (2 mL), conc. CH<sub>3</sub>COOH (1.2 mL), absolute EtOH (100 mL)), anisaldehyde solution (anisaldehyde (2.8 mL), conc. H<sub>2</sub>SO<sub>4</sub> (2 mL), conc. CH<sub>3</sub>COOH (1.2 mL), absolute EtOH (100 mL)), or ninhydrin solution (ninhydrin (200 mg), absolute EtOH (95 mL), 10% CH<sub>3</sub>COOH (5 mL)). For chromatography on silica gel, the flash chromatography technique was used with Merck silica gel 60 (230–400 mesh) and p.a. grade solvents.

The <sup>1</sup>H and <sup>13</sup>C NMR spectra were recorded in CDCl<sub>3</sub> or [D<sub>6</sub>]DMSO on Bruker Avance 500 or 250 spectrometers. The chemical shifts are reported in ppm relative to CHCl<sub>3</sub> or [D<sub>3</sub>]DMSO (δ = 7.26 and 2.50 ppm, respectively) for the <sup>1</sup>H NMR spectra and to CHCl<sub>3</sub> or [D<sub>5</sub>]DMSO (δ = 77.16 and 39.52 ppm, respectively) for the <sup>13</sup>C NMR spectra. High-resolution mass-spectrometric data were measured on a MicroMass LCT spectrometer and the IR spectra were recorded on Bruker Tensor 27 FTIR spectrometer. Melting points (mp) were determined in open capillaries on a Stuart Scientific Melting Point Apparatus SMP3.

**N-(2-Aminophenyl)benzamide (10a):** Et<sub>3</sub>N (2.6 mL, 18 mmol, 100 mol%) was added dropwise to a stirred solution of *ortho*-phenylenediamine (**8**; 4.00 g, 37 mmol, 200 mol%) in dichloromethane (100 mL) at room temperature. The solution was heated to reflux and benzoyl chloride (**9a**; 2.15 mL, 18 mmol, 100 mol%) in dichloromethane (80 mL) was added dropwise through a dropping funnel over 90 min. The solution was heated to reflux for 2 h and concentrated in vacuo. The residue was purified by flash chromatography (hexane/EtOAc 1:1) to afford amide **10a** (2.71 g, 69%) as a white solid.

R<sub>f</sub> (hexane/EtOAc 55:45) = 0.37; mp 149–151 °C; IR (film):  $\tilde{\nu}$  = 3401, 3269, 3059, 1642, 1602, 1577, 1525, 1499, 1450, 1315, 1290, 748 cm<sup>-1</sup>; <sup>1</sup>H NMR (500 MHz, [D<sub>6</sub>]DMSO): δ = 9.64 (s, 1H), 7.98 (d, 2H, J = 7.3 Hz), 7.59–7.56 (m, 1H), 7.53–7.50 (m, 2H), 7.18 (d, 1H, J = 7.5 Hz), 6.97 (td, 1H, J<sub>1</sub> = 8.0, J<sub>2</sub> = 1.5 Hz), 6.79 (dd, 1H, J<sub>1</sub> = 8.0, J<sub>2</sub> = 1.5 Hz), 6.60 (td, 1H, J<sub>1</sub> = 7., J<sub>2</sub> = 1.5 Hz), 4.88 ppm (s, 2H); <sup>13</sup>C NMR (125 MHz, [D<sub>6</sub>]DMSO): δ = 165.3, 143.1, 134.6, 131.3, 128.2, 127.7, 126.6, 126.4, 123.3, 116.2, 116.1 ppm; HRMS (ESI<sup>+</sup>): m/z calcd for [C<sub>13</sub>H<sub>12</sub>N<sub>2</sub>O<sub>2</sub>Na]<sup>+</sup>: 235.0847 [M + Na]<sup>+</sup>; found: 235.0843; Δ = -1.8 ppm (the NMR data is consistent with previous reports).<sup>[19]</sup>

**General procedure for the nitro-amide preparation:** Three different reported procedures were used.<sup>[20–22]</sup> Procedure A:<sup>[20]</sup> Et<sub>3</sub>N (130 mol%) was added to a stirred solution of *ortho*-nitroaniline (**11**) in THF at room temperature. Acyl chloride **9** was added dropwise through a dropping funnel. The solution was stirred at room temperature for 8 h and concentrated in vacuo. The residue was purified by flash chromatography (hexane/EtOAc 8:2) to afford the nitro-amide **12e**.

Procedure B:<sup>[21]</sup> Similar to procedure A, but a mixture of dichloromethane and pyridine (1:1) was used as a solvent, 4-dimethylaminopyridine (DMAP) was used (5 mol%) instead of Et<sub>3</sub>N, and the reaction was carried out at 0 °C for 2 h, allowed to warm to room temperature, and stirred for 4 h at room temperature. The solution was washed with 1 M HCl (4 × 50 mL), saturated NaHCO<sub>3</sub> (50 mL), and brine (50 mL) and dried over Na<sub>2</sub>SO<sub>4</sub>, filtered, and concentrated in vacuo. The residue was purified by flash chromatography to afford the nitro-amides **12d** and **12f**.

Procedure C:<sup>[22]</sup> Similar to procedure A, but neat pyridine was used as a solvent and Et<sub>3</sub>N was not used. The reaction time was 20 h. The solution was concentrated in vacuo; dissolved in CHCl<sub>3</sub>; washed with 1 M HCl (4×50 mL), water (2×50 mL), and brine (50 mL); dried over Na<sub>2</sub>SO<sub>4</sub>; filtered; and concentrated in vacuo. The residue was purified by flash chromatography (hexane/MtBE 1:1) to afford the nitro-amide **12c**.

**N-(2-Nitrophenyl)pivalamide (12e):** Procedure A: *R<sub>f</sub>* (hexane/EtOAc 8:2)=0.55; mp 42–44 °C; IR (film):  $\tilde{\nu}$ =3371, 2963, 1704, 1607, 1582, 1494, 1332, 1265, 1136, 744, 672 cm<sup>-1</sup>; <sup>1</sup>H NMR (500 MHz, CDCl<sub>3</sub>):  $\delta$ =10.72 (brs, 1H), 8.83 (dd, 1H, *J*<sub>1</sub>=8.6, *J*<sub>2</sub>=1.3 Hz), 8.22 (dd, 1H, *J*<sub>1</sub>=8.5, *J*<sub>2</sub>=1.6 Hz), 7.64 (dddd, 1H, *J*<sub>1</sub>=8.6, *J*<sub>2</sub>=7.2, *J*<sub>3</sub>=1.6, *J*<sub>4</sub>=0.4 Hz), 7.16 (ddd, 1H, *J*<sub>1</sub>=8.5, *J*<sub>2</sub>=7.2, *J*<sub>3</sub>=1.3 Hz), 1.36 ppm (s, 9H); <sup>13</sup>C NMR (125 MHz, CDCl<sub>3</sub>):  $\delta$ =178.0, 136.5, 136.1, 135.6, 125.9, 123.1, 122.3, 40.7, 27.6 ppm; HRMS (ESI<sup>-</sup>): *m/z* calcd for [C<sub>11</sub>H<sub>13</sub>N<sub>2</sub>O<sub>3</sub>]: 221.0926 [M-H]<sup>-</sup>; found: 221.0925;  $\Delta$ =-0.5 ppm.

**General procedure for the nitro-amide reduction:** This procedure was adapted from a previous report.<sup>[22]</sup> Pd/C catalyst (5%) was added to a stirred solution of amide derivative **12** in absolute EtOH under argon at room temperature. The reaction mixture was placed under vacuum and the atmosphere was replaced with hydrogen. The reaction mixture was stirred for 3 h at room temperature, the solution was filtered through a pad of celite with EtOAc, and the filtrate was concentrated in vacuo to afford amide **10**.

**N-(2-Aminophenyl)pivalamide (10e):** *R<sub>f</sub>* (hexane/EtOAc 8:2)=0.08; mp 143–145 °C; IR (film):  $\tilde{\nu}$ =3373, 3232, 2952, 1652, 1617, 1497, 1457, 1224, 744 cm<sup>-1</sup>; <sup>1</sup>H NMR (500 MHz, [D<sub>6</sub>]DMSO):  $\delta$ =8.73 (s, 1H), 7.01 (dd, 1H, *J*<sub>1</sub>=7.8, *J*<sub>2</sub>=1.2 Hz), 6.95–6.92 (m, 1H), 6.75 (dd, 1H, *J*<sub>1</sub>=8.0, *J*<sub>2</sub>=1.3 Hz), 6.57 (td, 1H, *J*<sub>1</sub>=7.5, *J*<sub>2</sub>=1.3 Hz), 4.63 (s, 2H), 1.24 ppm (s, 9H); <sup>13</sup>C NMR (125 MHz, [D<sub>6</sub>]DMSO):  $\delta$ =176.6, 143.0, 126.7, 126.2, 123.8, 116.4, 116.1, 38.7, 27.5 ppm; HRMS (ESI<sup>+</sup>): *m/z* calcd for [C<sub>11</sub>H<sub>17</sub>N<sub>2</sub>O]: 193.1335 [M+H]<sup>+</sup>; found: 193.1332;  $\Delta$ =-1.8 ppm.

**Dimethylpyridine-2,6-dicarboxylate:** The procedure was adapted from a previous report.<sup>[14]</sup> Conc. H<sub>2</sub>SO<sub>4</sub> (0.93 mL, 18 mmol, 35 mol%) was added dropwise to a stirred solution of pyridine-2,6-dicarboxylic acid (8.36 g, 50 mmol, 100 mol%) in MeOH (50 mL) at room temperature. The solution was heated to reflux for 48 h and the reaction was quenched by the addition of sat. NaHCO<sub>3</sub> (40 mL). The mixture was concentrated in vacuo and the residue was re-dissolved in CHCl<sub>3</sub> (50 mL). The product was washed with water (3×50 mL) and brine (50 mL), dried over Na<sub>2</sub>SO<sub>4</sub>, filtered, and concentrated in vacuo to afford the product (7.85 g, 80%) as a white solid.

*R<sub>f</sub>* (hexane/EtOAc 8:2)=0.67; mp 122–124 °C; IR (film):  $\tilde{\nu}$ =3063, 2969, 1739, 1571, 1449, 1434, 1288, 1241, 994, 951, 755, 694 cm<sup>-1</sup>; <sup>1</sup>H NMR (500 MHz, CDCl<sub>3</sub>):  $\delta$ =8.29 (d, 2H, *J*=7.8 Hz), 8.00 (dd, 1H, *J*<sub>1</sub>=*J*<sub>2</sub>=7.8 Hz), 4.01 ppm (s, 6H); <sup>13</sup>C NMR (125 MHz, CDCl<sub>3</sub>):  $\delta$ =165.2, 148.4, 138.4, 128.1, 53.3 ppm; HRMS (ESI<sup>+</sup>): *m/z* calcd for [C<sub>9</sub>H<sub>9</sub>NO<sub>4</sub>Na]: 218.0421 [M+Na]<sup>+</sup>; found: 218.0429;  $\Delta$ =-3.9 ppm (the NMR data is consistent with that reported previously).<sup>[23]</sup>

**6-(Methoxycarbonyl)pyridine-2-carboxylic acid (14):** The procedure was adapted from a previous report.<sup>[14]</sup> KOH (1.11 g, 20 mmol, 100 mol%) was dissolved in the minimal amount of water (0.5 mL) and was added to the cooled solution of dimethylpyridine-2,6-dicarboxylate (3.87 g, 20 mmol, 100 mol%) in MeOH (100 mL) at 0 °C. The solution was stirred at 0 °C for 2.5 h and warmed to room temperature. The mixture was concentrated in vacuo, and the residue was re-dissolved in water (80 mL) and washed with dichloromethane (2×50 mL). The aqueous layer was acidified with 1 M HCl (10 mL), and the product was extracted with EtOAc (4×50 mL).

The combined organic layers were washed with brine (70 mL), dried over Na<sub>2</sub>SO<sub>4</sub>, filtered, and concentrated in vacuo to afford the product **14** (2.67 g, 74%) as a white solid.

The product could not be visualized by TLC analysis; mp 147–149 °C; IR (film):  $\tilde{\nu}$ =1724, 1698, 1325, 1306, 1264, 1154, 1141, 750, 648 cm<sup>-1</sup>; <sup>1</sup>H NMR (500 MHz, [D<sub>6</sub>]DMSO):  $\delta$ =8.25–8.22 (m, 2H), 8.17 (dd, 1H, *J*<sub>1</sub>=7.9, *J*<sub>2</sub>=7.5 Hz), 3.92 ppm (s, 3H); <sup>13</sup>C NMR (125 MHz, [D<sub>6</sub>]DMSO):  $\delta$ =165.6, 164.7, 148.8, 147.6, 139.0, 127.8, 127.5, 52.6 ppm; HRMS (ESI<sup>-</sup>): *m/z* calcd for [C<sub>8</sub>H<sub>6</sub>NO<sub>4</sub>]: 180.0297 [M-H]<sup>-</sup>; found: 180.0296;  $\Delta$ =-0.2 ppm (the NMR data is consistent with that reported previously).<sup>[23]</sup>

**Methyl-6-(phenylcarbamoyl)pyridine-2-carboxylate (16):** *R<sub>f</sub>* (hexane/EtOAc 1:1)=0.46; mp 95–96 °C; IR (film):  $\tilde{\nu}$ =3487, 3447, 3253, 1721, 1678, 1598, 1532, 1495, 1433, 1327, 1300, 1238, 768, 735, 686 cm<sup>-1</sup>; <sup>1</sup>H NMR (500 MHz, [D<sub>6</sub>]DMSO):  $\delta$ =10.38 (s, 1H), 8.33–8.32 (m, 1H), 8.26–8.22 (m, 2H), 7.83 (d, 2H, *J*=8.5 Hz), 7.40–7.37 (m, 2H), 7.17–7.13 (m, 1H), 3.96 ppm (s, 3H); <sup>13</sup>C NMR (125 MHz, [D<sub>6</sub>]DMSO):  $\delta$ =164.6, 161.9, 150.4, 146.5, 139.6, 137.9, 128.8, 127.4, 125.6, 124.2, 120.2, 52.8 ppm; HRMS (ESI<sup>+</sup>): *m/z* calcd for [C<sub>14</sub>H<sub>12</sub>N<sub>2</sub>O<sub>3</sub>Na]: 279.0740 [M+Na]<sup>+</sup>; found: 279.0747;  $\Delta$ =2.5 ppm.

**6-(Phenylcarbamoyl)pyridine-2-carboxylic acid (17):** The procedure was adapted from a previous report.<sup>[14]</sup> LiOH (0.41 g, 17.1 mmol, 200 mol%) was added to a stirred solution of carboxylate **16** (2.18 g, 8.5 mmol, 100 mol%) in MeOH (100 mL) at room temperature. The mixture was stirred at room temperature for 1 h and MeOH was removed in vacuo. The residue was dissolved in water (100 mL) and acidified with 1 M HCl (30 mL). The product was extracted with EtOAc (2×100 mL and 2×50 mL), and the combined organic layers were dried over Na<sub>2</sub>SO<sub>4</sub>, filtered, and concentrated in vacuo to afford the product **17** (2.06 g, 100%) as a white solid.

The product could not be visualized by TLC analysis; mp 169–172 °C; IR (film):  $\tilde{\nu}$ =3330, 1698, 1664, 1600, 1535, 1445, 1322, 1242, 756, 686, 666, 644 cm<sup>-1</sup>; <sup>1</sup>H NMR (500 MHz, [D<sub>6</sub>]DMSO): 10.83 (s, 1H), 8.39 (d, 1H, *J*=7.5 Hz), 8.32–8.25 (m, 2H), 7.82 (d, 2H, *J*=8.1 Hz), 7.42 (t, 2H, *J*=7.8 Hz), 7.17 (t, 1H, *J*=7.4 Hz), 3.38 ppm (brs, 1H); <sup>13</sup>C NMR (125 MHz, [D<sub>6</sub>]DMSO):  $\delta$ =164.7, 161.4, 149.2, 146.1, 140.1, 137.9, 128.8, 127.0, 125.8, 124.4, 120.7 ppm; HRMS (ESI<sup>-</sup>): *m/z* calcd for [C<sub>13</sub>H<sub>9</sub>N<sub>2</sub>O<sub>3</sub>]: 241.0613 [M-H]<sup>-</sup>; found: 241.0611;  $\Delta$ =-1.0 ppm.

**6-((2-benzamidophenyl)carbamoyl)pyridine-2-carboxylic acid (19):** *N*-(2-Aminophenyl)benzamide **10a** (2.02 g, 9.52 mmol, 100 mol%) and HOBT (1.29 g, 9.52 mmol, 100 mol%) were added to a stirred solution of 6-(methoxycarbonyl)pyridine-2-carboxylic acid (**14**; 1.72 g, 9.52 mmol, 100 mol%) in THF (100 mL) at room temperature. The solution was cooled to 0 °C and stirred for 40 min. EDC (1.85 mL, 10.47 mmol, 110 mol%) and Et<sub>3</sub>N (1.46 mL, 10.47 mmol, 110 mol%) were added to the reaction mixture and the solution was stirred for further 45 min at 0 °C. The solution was warmed to room temperature, stirred for 20 h, and concentrated in vacuo. The residue was dissolved in dichloromethane (80 mL), washed with 1 M HCl (3×75 mL), sat. NaHCO<sub>3</sub> (100 mL), and water (80 mL) and dried over Na<sub>2</sub>SO<sub>4</sub>, filtered, and concentrated in vacuo to afford the product **18** (3.16 g, 89%) as a light-yellow solid. The product included small amounts of impurities, but it was used without further purification.

LiOH (0.11 g, 4.44 mmol, 200 mol%) was added to product **18** (0.83 g, 2.22 mmol, 100 mol%) in MeOH (40 mL) at room temperature. The formed suspension was stirred at room temperature for 1 h. The mixture was concentrated in vacuo and the residue was dissolved in water (50 mL). The solution was acidified with 1 M HCl

(10 mL) and the product was extracted with EtOAc (4×50 mL). The combined organic layers were dried over Na<sub>2</sub>SO<sub>4</sub>, filtered, and concentrated in vacuo to afford product **19** (0.76 g, 95%) as a white solid.

The product could not be visualized by TLC analysis; mp 208–210 °C; IR (film):  $\tilde{\nu}$  = 3270, 1753, 1673, 1645, 1601, 1519, 1484, 1452, 1339, 1317, 757, 742, 697, 678 cm<sup>-1</sup>; <sup>1</sup>H NMR (500 MHz, [D<sub>6</sub>]DMSO):  $\delta$  = 10.74 (s, 1H), 10.20 (s, 1H), 8.40 (dd, 1H, *J*<sub>1</sub> = 7.3 Hz, *J*<sub>2</sub> = 1.6 Hz), 8.30–8.24 (m, 2H), 8.04–8.02 (m, 2H), 7.98 (dd, 1H, *J*<sub>1</sub> = 8.0, *J*<sub>2</sub> = 1.5 Hz), 7.63 (dd, 1H, *J*<sub>1</sub> = 7.9, *J*<sub>2</sub> = 1.5 Hz), 7.60–7.57 (m, 1H), 7.52–7.49 (m, 1H), 7.36 (td, 1H, *J*<sub>1</sub> = 7.7, *J*<sub>2</sub> = 1.6 Hz), 7.31 ppm (td, 1H, *J*<sub>1</sub> = 7.7, *J*<sub>2</sub> = 1.6 Hz); <sup>13</sup>C NMR (125 MHz, [D<sub>6</sub>]DMSO):  $\delta$  = 166.2, 165.0, 161.6, 149.2, 146.8, 140.1, 134.2, 131.74, 131.70, 130.4, 128.4, 127.9, 127.3, 126.7, 126.1, 125.5, 125.4, 124.4 ppm; HRMS (ESI<sup>-</sup>): *m/z* calcd for [C<sub>20</sub>H<sub>14</sub>N<sub>3</sub>O<sub>4</sub>]: 360.0984 [M-H]<sup>-</sup>; found: 360.0978;  $\Delta$  = -1.8 ppm.

**General procedure for the coupling reactions:**<sup>[24]</sup> HOBT and the amide derivative were added to a stirred solution of an asymmetric pyridine carboxylic acid in THF at room temperature. The mixture was cooled to 0 °C and stirred for 30 min. EDC and Et<sub>3</sub>N were added to the reaction mixture and the solution was stirred for further 30 min at 0 °C. The solution was warmed to room temperature, stirred overnight, and concentrated in vacuo. The residue was dissolved in EtOAc, washed with several portions of 1 M HCl and finally with brine, dried over Na<sub>2</sub>SO<sub>4</sub>, filtered, and concentrated in vacuo to afford the product.

#### N<sup>2</sup>-(2-Benzamidophenyl)-N<sup>6</sup>-phenylpyridine-2,6-dicarboxamide

**(2):** Prepared according to the general procedure for a coupling reaction with carboxylic acid **17** (1.080 g, 4.46 mmol, 100 mol%) in THF (20 mL), HOBT (0.603 g, 4.46 mmol, 100 mol%), amide **10a** (0.947 g, 4.46 mmol, 100 mol%), EDC (0.84 mL, 4.73 mmol, 106 mol%), Et<sub>3</sub>N (0.66 mL, 4.73 mmol, 106 mol%), and THF (30 mL) to yield the product (1.843 g, 95%) as a white solid. *R*<sub>f</sub> (hexane/EtOAc 1:1) = 0.41; mp 229–232 °C; IR (film):  $\tilde{\nu}$  = 3316, 3232, 1677, 1660, 1645, 1597, 1528, 1445, 1312, 750, 706 cm<sup>-1</sup>; <sup>1</sup>H NMR (500 MHz, [D<sub>6</sub>]DMSO):  $\delta$  = 11.14 (s, 1H), 10.76 (s, 1H), 10.34 (s, 1H), 8.40 (td, 2H, *J*<sub>1</sub> = 7.7, *J*<sub>2</sub> = 1.1 Hz), 8.31–8.28 (m, 1H), 7.89–7.86 (m, 3H), 7.77 (d, 2H, *J* = 8.1 Hz), 7.64 (dd, 1H, *J*<sub>1</sub> = 7.8, *J*<sub>2</sub> = 1.4 Hz), 7.45–7.33 (m, 5H), 7.27 (t, 2H, *J* = 7.8 Hz), 7.18–7.15 ppm (m, 1H); <sup>13</sup>C NMR (125 MHz, [D<sub>6</sub>]DMSO):  $\delta$  = 166.4, 161.3, 148.6, 148.5, 140.1, 137.7, 134.0, 131.7, 131.0, 128.6, 128.2, 127.6, 125.94, 125.88, 125.6, 125.2, 125.1, 124.4, 121.0 ppm; HRMS (ESI<sup>+</sup>): *m/z* calcd for [C<sub>26</sub>H<sub>20</sub>N<sub>4</sub>O<sub>3</sub>Na]: 459.1433 [M+Na]<sup>+</sup>; found: 459.1426;  $\Delta$  = -1.6 ppm.

**N<sup>2</sup>-(2-Benzamidophenyl)-N<sup>6</sup>-(2-(4-cyanobenzamido)phenyl)pyridine-2,6-dicarboxamide (3):** Prepared according to the general procedure for a coupling reaction with carboxylic acid **19** (359 mg, 1.00 mmol, 100 mol%), amide **10b** (237 mg, 1.00 mmol, 100 mol%), HOBT (135 mg, 1.00 mmol, 100 mol%), EDC (0.19 mL, 1.10 mmol, 110 mol%), Et<sub>3</sub>N (0.15 mL, 1.10 mmol, 110 mol%), and THF (50 mL) to yield the product (544 mg, 94%) as a light-brown solid. *R*<sub>f</sub> (hexane/EtOAc 3:7) = 0.56; mp 252–254 °C; IR (film):  $\tilde{\nu}$  = 2230, 1667, 1599, 1515, 1480, 1441, 1306, 754 cm<sup>-1</sup>; <sup>1</sup>H NMR (500 MHz, [D<sub>6</sub>]DMSO):  $\delta$  = 11.00 (s, 1H), 10.85 (s, 1H), 10.38 (s, 1H), 10.29 (s, 1H), 8.38–8.36 (m, 2H), 8.30–8.27 (m, 1H), 7.91 (d, 2H, *J* = 8.4 Hz), 7.77–7.75 (m, 1H), 7.72 (d, 2H, *J* = 7.2 Hz), 7.65–7.63 (m, 2H), 7.59 (d, 2H, *J* = 8.5 Hz), 7.56–7.54 (m, 1H), 7.45–7.42 (m, 1H), 7.39–7.31 (m, 4H), 7.22–7.19 ppm (m, 2H); <sup>13</sup>C NMR (125 MHz, [D<sub>6</sub>]DMSO):  $\delta$  = 166.1, 164.5, 161.3, 161.1, 148.33, 148.29, 140.3, 138.2, 133.7, 131.9, 131.7, 131.1, 130.8, 130.7, 130.5, 128.3, 128.1, 127.7, 126.2, 126.0, 125.7, 125.6, 125.5, 125.2, 125.09, 125.06, 125.0, 118.1, 113.7 ppm; HRMS (ESI<sup>+</sup>): *m/z* calcd for [C<sub>34</sub>H<sub>24</sub>N<sub>6</sub>O<sub>4</sub>Na]: 603.1751 [M+Na]<sup>+</sup>; found: 603.1745;  $\Delta$  = -1.0 ppm.

**N<sup>2</sup>-(2-Benzamidophenyl)-N<sup>6</sup>-(2-(4-methoxybenzamido)phenyl)pyridine-2,6-dicarboxamide (4):** Prepared according to the general procedure for a coupling reaction with carboxylic acid **19** (183 mg, 0.51 mmol, 100 mol%), amide **10c** (136 mg, 0.56 mmol, 110 mol%), HOBT (83 mg, 0.56 mmol, 110 mol%), EDC (0.11 mL, 0.61 mmol, 120 mol%), Et<sub>3</sub>N (0.09 mL, 0.61 mmol, 120 mol%), and THF (50 mL) to yield the product (90 mg, 30%) as a white solid. *R*<sub>f</sub> (hexane/EtOAc 3:7) = 0.51; mp 172–174 °C; IR (film):  $\tilde{\nu}$  = 3345, 1698, 1682, 1648, 1633, 1605, 1509, 1439, 1307, 1258, 755 cm<sup>-1</sup>; <sup>1</sup>H NMR (500 MHz, [D<sub>6</sub>]DMSO):  $\delta$  = 11.04 (s, 1H), 10.98 (s, 1H), 10.22 (s, 1H), 10.11 (s, 1H), 8.38–8.36 (m, 2H), 8.30–8.27 (m, 1H), 7.76 (dd, 2H, *J*<sub>1</sub> = 8.2, *J*<sub>2</sub> = 1.0 Hz), 7.73–7.71 (m, 4H), 7.68–7.67 (m, 1H), 7.62–7.61 (m, 1H), 7.44–7.41 (m, 1H), 7.37–7.32 (m, 4H), 7.20 (t, 2H, *J* = 7.8 Hz), 6.70 (d, 2H, *J* = 8.9 Hz), 3.74 ppm (s, 3H); <sup>13</sup>C NMR (125 MHz, [D<sub>6</sub>]DMSO):  $\delta$  = 166.0, 165.5, 161.9, 161.3, 161.2, 148.3, 148.2, 140.4, 134.0, 131.6, 131.10, 131.07, 130.8, 129.5, 128.1, 127.5, 125.9, 125.9, 125.8, 125.7, 125.6, 125.3, 125.11, 125.07, 113.3, 55.3 ppm; HRMS (ESI<sup>+</sup>): *m/z* calcd for [C<sub>34</sub>H<sub>27</sub>N<sub>5</sub>O<sub>5</sub>Na]: 608.1904 [M+Na]<sup>+</sup>; found: 608.1903;  $\Delta$  = -0.2 ppm.

**N<sup>2</sup>-(2-Acetamidophenyl)-N<sup>6</sup>-(2-benzamidophenyl)pyridine-2,6-dicarboxamide (5):** Prepared according to the general procedure for a coupling reaction with carboxylic acid **19** (479 mg, 1.33 mmol, 100 mol%), amide **10d** (230 mg, 1.53 mmol, 115 mol%), HOBT (207 mg, 1.53 mmol, 115 mol%), EDC (0.30 mL, 1.66 mmol, 125 mol%), Et<sub>3</sub>N (0.23 mL, 1.66 mmol, 125 mol%), and THF (70 mL) to yield the product (588 mg, 90%) as a white solid. *R*<sub>f</sub> (hexane/EtOAc 2:8) = 0.55; mp 227–229 °C; IR (film):  $\tilde{\nu}$  = 3227, 3037, 1693, 1666, 1646, 1597, 1511, 1481, 1445, 1311, 754, 705 cm<sup>-1</sup>; <sup>1</sup>H NMR (500 MHz, CDCl<sub>3</sub>):  $\delta$  = 11.25 (s, 1H), 11.12 (s, 1H), 9.65 (s, 1H), 9.07 (s, 1H), 8.47 (d, 1H, *J* = 7.6 Hz), 8.43 (d, 1H, *J* = 7.8 Hz), 8.11 (t, 1H, *J* = 7.8 Hz), 7.94 (d, 1H, *J* = 7.5 Hz), 7.80 (d, 2H, *J* = 7.5 Hz), 7.72–7.69 (m, 2H), 7.40 (t, 1H, *J* = 7.4 Hz), 7.28–7.24 (m, 3H), 7.22–7.16 (m, 3H), 7.08–7.05 (m, 1H), 1.71 ppm (s, 3H); <sup>13</sup>C NMR (125 MHz, CDCl<sub>3</sub>):  $\delta$  = 170.8, 166.4, 162.7, 161.7, 149.0, 148.4, 139.6, 133.8, 132.1, 131.1, 130.8, 130.2, 129.7, 128.7, 127.5, 126.66, 126.64, 126.33, 126.25, 125.9, 125.7, 125.53, 125.51, 125.1, 124.8, 23.4 ppm; HRMS (ESI<sup>+</sup>): *m/z* calcd for [C<sub>28</sub>H<sub>23</sub>N<sub>5</sub>O<sub>4</sub>Na]: 516.1627 [M+Na]<sup>+</sup>; found: 516.1642;  $\Delta$  = -3.0 ppm.

**N<sup>2</sup>-(2-Benzamidophenyl)-N<sup>6</sup>-(2-isobutyramidophenyl)pyridine-2,6-dicarboxamide (6):** Prepared according to the general procedure for a coupling reaction with carboxylic acid **19** (310 mg, 0.85 mmol, 100 mol%), amide **10e** (170 mg, 0.95 mmol, 110 mol%), HOBT (129 mg, 0.95 mmol, 110 mol%), EDC (0.19 mL, 1.05 mmol, 120 mol%), Et<sub>3</sub>N (0.15 mL, 1.05 mmol, 120 mol%), and THF (50 mL) to yield the product (383 mg, 77%) as a white solid. *R*<sub>f</sub> (hexane/EtOAc 3:7) = 0.50; mp 192–193 °C; IR (film):  $\tilde{\nu}$  = 1650, 1599, 1513, 1480, 1450, 1302, 750 cm<sup>-1</sup>; <sup>1</sup>H NMR (500 MHz, CDCl<sub>3</sub>):  $\delta$  = 11.06 (s, 1H), 10.97 (s, 1H), 9.54 (s, 1H), 8.72 (s, 1H), 8.46 (d, 1H, *J* = 7.7 Hz), 8.44 (d, 1H, *J* = 7.8 Hz), 8.12 (t, 1H, *J* = 7.8 Hz), 7.87 (dd, 1H, *J*<sub>1</sub> = 7.8, *J*<sub>2</sub> = 1.6 Hz), 7.80–7.77 (m, 3H), 7.59 (d, 1H, *J* = 7.7 Hz), 7.34 (t, 1H, *J* = 7.4 Hz), 7.20–7.10 (m, 5H), 7.05–7.02 (m, 1H), 2.40 (septet, 1H, *J* = 6.9 Hz), 0.89 ppm (d, 1H, *J* = 6.9 Hz); <sup>13</sup>C NMR (125 MHz, CDCl<sub>3</sub>):  $\delta$  = 177.6, 166.6, 162.1, 162.0, 148.7, 148.6, 139.7, 133.8, 132.0, 130.7, 130.4, 130.1, 128.7, 128.6, 127.6, 127.5, 126.6, 126.5, 126.1, 125.6, 125.53, 125.45, 125.2, 124.9, 36.1, 19.3 ppm; HRMS (ESI<sup>+</sup>): *m/z* calcd for [C<sub>30</sub>H<sub>28</sub>N<sub>5</sub>O<sub>4</sub>]: 522.2135 [M+H]<sup>+</sup>; found: 522.2135;  $\Delta$  = -0.9 ppm.

**N<sup>2</sup>-(2-Benzamidophenyl)-N<sup>6</sup>-(2-pivalamidophenyl)pyridine-2,6-dicarboxamide (7):** Prepared according to the general procedure for a coupling reaction with carboxylic acid **19** (340 mg, 0.95 mmol, 100 mol%), amide **10f** (200 mg, 1.04 mmol, 110 mol%), HOBT (141 mg, 1.04 mmol, 110 mol%), EDC (0.20 mL, 1.13 mmol, 120 mol%), Et<sub>3</sub>N (0.16 mL, 1.13 mmol, 120 mol%), and THF (50 mL)

to yield the product (502 mg, 99%) as a white solid.  $R_f$  (hexane/EtOAc 1:1)=0.37; mp 210–212 °C; IR (film):  $\tilde{\nu}$ =1691, 1676, 1638, 1601, 1524, 1481, 756, 707  $\text{cm}^{-1}$ ;  $^1\text{H}$  NMR (500 MHz,  $[\text{D}_6]\text{DMSO}$ ):  $\delta$ =11.04 (s, 1H), 10.88 (s, 1H), 10.20 (s, 1H), 9.05 (s, 1H), 8.41 (dd, 1H,  $J_1=7.7$ ,  $J_2=1.2$  Hz), 8.38 (dd, 1H,  $J_1=7.8$ ,  $J_2=1.2$  Hz), 8.31 (dd, 1H,  $J_1=J_2=7.8$  Hz), 7.87 (dd, 1H,  $J_1=7.9$ ,  $J_2=1.5$  Hz), 7.75 (dd, 2H,  $J_1=8.3$ ,  $J_2=1.2$  Hz), 7.62 (dd, 1H,  $J_1=7.9$ ,  $J_2=1.3$  Hz), 7.56 (dd, 1H,  $J_1=7.8$ ,  $J_2=1.7$  Hz), 7.52 (dd, 1H,  $J_1=7.7$ ,  $J_2=1.7$  Hz), 7.44–7.41 (m, 1H), 7.37 (td, 1H,  $J_1=7.7$ ,  $J_2=1.6$  Hz), 7.33–7.25 (m, 3H), 7.22–7.19 (m, 2H), 1.03 ppm (s, 9H);  $^{13}\text{C}$  NMR (125 MHz,  $[\text{D}_6]\text{DMSO}$ ):  $\delta$ =176.8, 166.1, 161.5, 161.3, 148.5, 148.1, 140.4, 133.8, 131.63, 131.62, 131.0, 130.9, 130.4, 128.1, 127.5, 126.00, 125.98, 125.9, 125.8, 125.6, 125.4, 125.3, 125.2, 125.1, 125.0, 38.8, 26.9 ppm; HRMS (ESI+):  $m/z$  calcd for  $[\text{C}_{31}\text{H}_{29}\text{N}_5\text{O}_4\text{Na}]$ : 588.2111  $[\text{M}+\text{Na}]^+$ ; found: 588.2117;  $\Delta$ =0.9 ppm.

### Crystallographic analysis

The compounds were dissolved in solvents of analytical purity (foldamer 2: acetone, MeCN/ dimethylacetamide (DMA), DMF; foldamer 3: MeCN, EtOAc; foldamer 5: acetone; foldamer 6: EtOAc, toluene; foldamer 7: acetone; see the Supporting Information for details) and allowed to evaporate at room temperature until crystals formed. Aliquots of 10–50 mg of the compounds and up to 6 mL of the solvents were used in the crystallization experiments. Heating and stirring were used to help the dissolving process.

Single-crystal X-ray diffraction data was collected on a Bruker Nonius KappaCCD diffractometer at 173 K with a Bruker AXS APEX II CCD detector and graphite-monochromated  $\text{Cu}_{\text{K}\alpha}$  radiation ( $\lambda=1.54178$  Å). The structures were solved by using direct methods and refined by using Fourier techniques with the SHELX-97 software package.<sup>[25]</sup> Multiscan absorption correction was applied to all structures with Denzo-SMN 1997.<sup>[26]</sup> All the non-hydrogen atoms were refined anisotropically. The hydrogen atoms were placed in their idealized positions, except for the N–H hydrogen atoms that were found from the electron-density map and included in the structure-factor calculations. Isotropic temperature factor of 1.2 was used to refine the hydrogen atoms. Details of the crystal data and the refinement are presented in Tables 2 and 3 in the Supporting Information.

CCDC 1038215 (2-@-Form I), CCDC 1038216 (2-S-MeCN), CCDC 1038217 (2-@-S-DMF), CCDC 1038218 (3-@<sub>2</sub>-Form I), CCDC 1038219 (3-S<sub>1</sub>-EtOAc), CCDC 1038220 (5-S<sub>1</sub>-Form I), CCDC 1038221 (6-@<sub>2</sub>-Form I), CCDC 1038222 (6-S<sub>1</sub>-Form II), and CCDC 1038223 (7-S<sub>2</sub>-Form I) contain the supplementary crystallographic data for this paper. These data can be obtained free of charge from The Cambridge Crystallographic Data Centre through [www.ccdc.cam.ac.uk/data\\_request/cif](http://www.ccdc.cam.ac.uk/data_request/cif).

### Computational approach

The geometries of the stationary points were optimized by using the density-functional theory (DFT) at the  $\omega\text{B97X-D}/6\text{-}311\text{G(d,p)}$  level. Herein,  $\omega\text{B97X-D}$  denotes the long-range corrected hybrid density functional with damped atom–atom dispersion corrections developed by Chai and Head-Gordon.<sup>[27,28]</sup> This functional is a very promising DFT method<sup>[29]</sup> that yields reasonably accurate data for general main-group thermochemistry, kinetics, and noncovalent interactions (all of which are relevant to the present work). The initial structures for the geometry optimizations were obtained from a Monte Carlo conformational search by using the OPLS 2005 force fields as implemented in the MacroModel software.<sup>[30]</sup> The preliminary conformational analysis involved a systematic search

and DFT potential-energy surface scans along specific dihedral angles.

Normal coordinate analysis was carried out at the  $\omega\text{B97X-D}/6\text{-}311\text{G(d,p)}$  level of theory for all the optimized structures. The results were utilized to verify the nature of the stationary points (i.e. minima) and to estimate the zero-point energies and the thermal and entropic contributions to the Gibbs free energies. For each located structure, additional single-point energy calculations were performed at the  $\omega\text{B97X-D}/6\text{-}311 + \text{G(3df,3pd)}$  level to increase the accuracy of the electronic-structure predictions. In all the DFT calculations, the ultrafine integration grid was employed, as implemented in the Gaussian09 package.<sup>[31]</sup>

The thermochemical data were obtained within the ideal-gas (i.e., rigid rotor) harmonic-oscillator approximation for  $T=298.15$  K and  $P=1$  atm. The solvation free energies (solvent= $\text{CHCl}_3$ ) were estimated at the  $\omega\text{B97X-D}/6\text{-}311\text{G(d,p)}$  level by using the integral-equation-formalism variant of the polarizable-continuum model (IEFPCM).<sup>[32]</sup> The atomic radii and nonelectrostatic terms in the IEFPCM calculations were those introduced recently by Truhlar and co-workers (SMD solvation model).<sup>[33]</sup>

### Acknowledgements

We thank the Finnish Cultural Foundation, University of Jyväskylä, Academy of Finland (Grant no. 259532), and the Hungarian Scientific Research Fund (OTKA, grant NN-82955) for financial support.

**Keywords:** crystal growth • foldamers • protein folding • hydrogen bonds • oligomerization

- [1] D. Blow, *Structure* **2000**, *8*, R77–R81.
- [2] P. M. Pihko, S. Rapakko, R. K. Wierenga in *Hydrogen Bonding in Organic Synthesis* (Ed. P. M. Pihko), Wiley-VCH, Weinheim, **2009**, pp. 43–72.
- [3] For a discussion, see: a) R. R. Knowles, E. N. Jacobsen, *Proc. Natl. Acad. Sci. USA* **2010**, *107*, 20678; for a recent example of a synthetic oxyanion mimic, see: b) E. V. Beletskiy, J. Schmidt, X.-B. Wang, S. R. Kass, *J. Am. Chem. Soc.* **2012**, *134*, 18534–18537; c) see also ref. [2]; d) B. Kótai, G. Kardos, A. Hamza, V. Farkas, I. Pápai, T. Soós, *Chem. Eur. J.* **2014**, *20*, 5631–5639.
- [4] a) S. H. Gellman, *Acc. Chem. Res.* **1998**, *31*, 173–180; b) D. J. Hill, M. J. Mio, R. B. Prince, T. S. Hughes, J. S. Moore, *Chem. Rev.* **2001**, *101*, 3893–4011; c) S. Hecht, I. Huc, *Foldamers: Structure, Properties and Applications*, Wiley-VCH, Weinheim, **2007**; d) D.-W. Zhang, X. Zhao, Z.-T. Li, *Acc. Chem. Res.* **2014**, *47*, 1961–1970; e) G. Guichard, I. Huc, *Chem. Commun.* **2011**, *47*, 5933–5941.
- [5] a) D.-W. Zhang, X. Zhao, J.-L. Hou, Z.-T. Li, *Chem. Rev.* **2012**, *112*, 5271–5316; b) I. Huc, *Eur. J. Org. Chem.* **2004**, 17–29; c) B. Gong, *Chem. Eur. J.* **2001**, *7*, 4336–4342; d) A. R. Sanford, K. Yamato, X. Yang, L. Yuan, Y. Han, B. Gong, *Eur. J. Biochem.* **2004**, *271*, 1416–1425; e) K. Yamato, M. Kline, B. Gong, *Chem. Commun.* **2012**, *48*, 12142–12158.
- [6] a) V. Berl, I. Huc, R. G. Khoury, J.-M. Lehn, *Chem. Eur. J.* **2001**, *7*, 2798–2809; b) V. Berl, I. Huc, R. G. Khoury, J.-M. Lehn, *Chem. Eur. J.* **2001**, *7*, 2810–2820; c) I. Huc, V. Maurizot, H. Gornitzka, J.-M. Léger, *Chem. Commun.* **2002**, *6*, 578–579; d) B. Babbiste, J. Zhu, D. Haldar, B. Kauffmann, J.-M. Léger, I. Huc, *Chem. Asian J.* **2010**, *5*, 1364–1375.
- [7] a) Y. Hamuro, S. J. Geib, A. D. Hamilton, *Angew. Chem. Int. Ed. Engl.* **1994**, *33*, 446–448; *Angew. Chem.* **1994**, *106*, 465–467; b) Y. Hamuro, S. J. Geib, A. D. Hamilton, *J. Am. Chem. Soc.* **1996**, *118*, 7529–7541; c) Y. Hamuro, S. J. Geib, A. D. Hamilton, *J. Am. Chem. Soc.* **1997**, *119*, 10587–10593.
- [8] a) H. Jiang, J.-M. Léger, I. Huc, *J. Am. Chem. Soc.* **2003**, *125*, 3448–3449; b) E. R. Gillies, C. Dolain, J.-M. Léger, I. Huc, *J. Org. Chem.* **2006**, *71*, 7931–7931; c) N. Delsuc, J.-M. Léger, S. Massip, I. Huc, *Angew. Chem. Int.*

- Ed. **2007**, *46*, 214–217; *Angew. Chem.* **2007**, *119*, 218–221; d) D. Sánchez-García, B. Kauffmann, T. Kawanami, H. Ihara, M. Takafuji, M.–H. Delville, I. Huc, *J. Am. Chem. Soc.* **2009**, *131*, 8642–8648.
- [9] Y. Ferrand, A. M. Kendhale, J. Garric, B. Kauffman, I. Huc, *Angew. Chem. Int. Ed.* **2010**, *49*, 1778–1781; *Angew. Chem.* **2010**, *122*, 1822–1825.
- [10] a) J. T. Ernst, J. Becerril, H. S. Park, H. Yin, A. D. Hamilton, *Angew. Chem. Int. Ed.* **2003**, *42*, 535–539; *Angew. Chem.* **2003**, *115*, 553–557; L. A. Estroff, C. D. Incarvato, A. D. Hamilton, *J. Am. Chem. Soc.* **2004**, *126*, 2–3; I. Saraogi, C. D. Incarvato, A. D. Hamilton, *Angew. Chem. Int. Ed.* **2008**, *47*, 9691–9694; *Angew. Chem.* **2008**, *120*, 9837–9840; b) C. Li, S.-F. Ren, J.-L. Hou, H.-P. Yi, S.-Z. Zhu, X.-K. Jiang, Z.-T. Li, *Angew. Chem. Int. Ed.* **2005**, *44*, 5725–5729; *Angew. Chem.* **2005**, *117*, 5871–5875; c) J.-L. Hou, X.-B. Shao, G.-J. Chen, Y.-X. Zhou, X.-K. Jiang, Z.-T. Li, *J. Am. Chem. Soc.* **2004**, *126*, 12386–12394; H.-P. Yi, X.-B. Shao, J.-L. Hou, C. Li, X.-K. Jiang, Z.-T. Li, *New J. Chem.* **2005**, *29*, 1213–1218; H.-P. Yi, C. Li, J.-L. Hou, X.-K. Jiang, Z.-T. Li, *Tetrahedron* **2005**, *61*, 7974–7980; d) J. Zhu, R. D. Parra, H. Zeng, E. Skrzypczak-Jankun, X. C. Zeng, B. Gong, *J. Am. Chem. Soc.* **2000**, *122*, 4219–4220.
- [11] K. Mitsui, S. A. Hyatt, D. A. Turner, C. M. Hadad, J. R. Parquette, *Chem. Commun.* **2009**, 3261–3263; b) N. T. Salzameda, D. A. Lightner, *Monatsh. Chem.* **2007**, *138*, 237–244.
- [12] a) I. Pápai, A. Hamza, P. M. Pihko, R. K. Wierenga, *Chem. Eur. J.* **2011**, *17*, 2859–2866; b) for a seminal study of the preferred hydrogen-bond orientation in oxanion holes, see: L. Simón, J. M. Goodman, *J. Org. Chem.* **2010**, *75*, 1831.
- [13] A. Suhonen, E. Nauha, K. Salorinne, K. Helttunen, M. Nissinen, *CrystEngComm* **2012**, *14*, 7398–7407.
- [14] C. Schmuck, U. Machon, *Chem. Eur. J.* **2005**, *11*, 1109–1118.
- [15] The RDG data were computed by using the NCIPLOT program; for a basic reference, see: a) E. R. Johnson, S. Keinan, P. Mori-Sánchez, J. Contreras-García, A. J. Cohen, W. Yang, *J. Am. Chem. Soc.* **2010**, *132*, 6498; b) J. Contreras-García, E. R. Johnson, S. Keinan, R. Chaudret, J. Piquemal, D. N. Beratan, W. Yang, *J. Chem. Theory Comput.* **2011**, *7*, 625.
- [16] RDG isosurface plots were visualized by using the visual molecular dynamics (VMD) program: W. Humphrey, A. Dalke, K. Schulten, *J. Molec. Graphics* **1996**, *14*, 33.
- [17] See the Supporting Information for additional overlay structures and the distances of the intramolecular aromatic interactions in the XRD structures.
- [18] The details of the effects of solvation and crystal packing will be discussed elsewhere; A. Suhonen, M. Kortelainen, E. Nauha, S. Yliniemelä-Sipari, P. Pihko and M. Nissinen, *Manuscript in preparation*.
- [19] H. Zhao, H. Fu, R. Qiao, *J. Org. Chem.* **2010**, *75*, 3311–3316.
- [20] Y.-W. Legrand, M. Gray, G. Cooke, V. M. Rotello, *J. Am. Chem. Soc.* **2003**, *125*, 15789–15795.
- [21] J. Duchek, A. Vasella, *Helv. Chim. Acta* **2011**, *94*, 977–986.
- [22] H. Koshio, F. Hirayama, T. Ishihara, R. Shiraki, T. Shigenaga, Y. Taniuchi, K. Sato, Y. Moritani, Y. Iwatsuki, S. Kaku, N. Katayama, T. Kawasaki, Y. Matsumoto, S. Sakamoto, S. Tsukamoto, *Bioorg. Med. Chem.* **2005**, *13*, 1305–1323.
- [23] W. Ong, H. Zhao, Z. Du, J. Z. Y. Yeh, C. Ren, L. Z. W. Tan, K. Zhang, H. Zeng, *Chem. Commun.* **2011**, *47*, 6416–6418.
- [24] F. Stomeo, C. Lincheneau, J. P. Leonard, J. E. O'Brien, R. D. Peacock, C. P. McCoy, T. Gunnlaugsson, *J. Am. Chem. Soc.* **2009**, *131*, 9636–9637.
- [25] G. M. Sheldrick, *Acta Crystallogr. Sect. A* **2008**, *64*, 112–122.
- [26] Z. Otwinowski, D. Borek, W. Majewski, W. Minor, *Acta Crystallogr. Sect. A* **2003**, *59*, 228–234.
- [27] a) J.-D. Chai, M. Head-Gordon, *Phys. Chem. Chem. Phys.* **2008**, *10*, 6615–6620; b) J.-D. Chai, M. Head-Gordon, *J. Chem. Phys.* **2008**, *128*, 084106/1–084106/15.
- [28] a) R. Krishnan, J. S. Binkley, R. Seeger, J. A. Pople, *J. Chem. Phys.* **1980**, *72*, 650–654; b) A. D. McLean, G. S. Chandler, *J. Chem. Phys.* **1980**, *72*, 5639–5648; c) T. Clark, J. Chandrasekhar, G. W. Spitznagel, P. v. R. Schleyer, *J. Comput. Chem.* **1983**, *4*, 294–301; d) M. J. Frisch, J. A. Pople, J. S. Binkley, *J. Chem. Phys.* **1984**, *80*, 3265–3269.
- [29] L. Goerigk, S. Grimme, *Phys. Chem. Chem. Phys.* **2011**, *13*, 6670–6688.
- [30] Schrödinger Release 2013–3: MacroModel, version 10.2, Schrödinger, LLC, New York, NY, **2013**.
- [31] Gaussian 09, Revision A.02, M. J. Frisch, G. W. Trucks, H. B. Schlegel, G. E. Scuseria, M. A. Robb, J. R. Cheeseman, G. Scalmani, V. Barone, B. Mennucci, G. A. Petersson, H. Nakatsuji, M. Caricato, X. Li, H. P. Hratchian, A. F. Izmaylov, J. Bloino, G. Zheng, J. L. Sonnenberg, M. Hada, M. Ehara, K. Toyota, R. Fukuda, J. Hasegawa, M. Ishida, T. Nakajima, Y. Honda, O. Kitao, H. Nakai, T. Vreven, J. A. Montgomery, Jr., J. E. Peralta, F. Ogliaro, M. Bearpark, J. J. Heyd, E. Brothers, K. N. Kudin, V. N. Staroverov, R. Kobayashi, J. Normand, K. Raghavachari, A. Rendell, J. C. Burant, S. S. Iyengar, J. Tomasi, M. Cossi, N. Rega, J. M. Millam, M. Klene, J. E. Knox, J. B. Cross, V. Bakken, C. Adamo, J. Jaramillo, R. Gomperts, R. E. Stratmann, O. Yazyev, A. J. Austin, R. Cammi, C. Pomelli, J. W. Ochterski, R. L. Martin, K. Morokuma, V. G. Zakrzewski, G. A. Voth, P. Salvador, J. J. Dannenberg, S. Dapprich, A. D. Daniels, Ö. Farkas, J. B. Foresman, J. V. Ortiz, J. Cioslowski, D. J. Fox, Gaussian, Inc., Wallingford CT, **2009**.
- [32] J. Tomasi, B. Mennucci, E. Cancès, *J. Mol. Struct.* **1999**, *464*, 211–226.
- [33] A. V. Marenich, C. J. Cramer, D. G. Truhlar, *J. Phys. Chem. B* **2009**, *113*, 6378–6396.

Received: December 17, 2014  
Published online on May 12, 2015